Journal of Materials Chemistry C

ARTICLE

Combinatorial Synthesis and Screening of (Ba,Sr)(Ti,Mn)O_3 Thin Films for Optimization of Tunable Co-Planar Waveguides

Received 00th January 20xx,
Accepted 00th January 20xx

DOI: 10.1039/x0xx00000x

www.rsc.org/

Ioanna Bakaimi,[a] Xingli He,[b] Samuel Guerin,[c] Nur Zatil Ismah Hashim, [b] Qi Luo,[d] Ian Reaney,[e] Steven Gao,[d] Brian E. Hayden*[a,c] and C.H. Kees de Groot*[b]

The identification and optimization of tunable dielectric materials exhibiting low loss characteristics in the GHz frequencies are essential in the development of low power devices for microwave applications. We have applied a combinatorial synthetic methodology employing multiple atomic evaporative sources to produce compositional gradient thin films (Ba,Sr)(Ti,Mn)O_3 perovskites. High throughput screening chips of both capacitive and waveguide structures are used to measure the compositional dependence of the dielectric properties of fully characterised thin film materials. The co-planar waveguides are shown to allow measurements at frequencies exceeding 10 GHz. Using the methodology, we have identified (Ba,Sr)(Ti,Mn)O_3 compositions which exhibit good tunability with low losses at microwave frequencies: For a single device with a 10 V DC bias one can achieve a 12 degree phase shift with excellent transmission characteristics, and insertion loss of ~3.2 dB. We show that small changes in composition can result in significant change in dielectric characteristics and device performance, and that the experimental protocol developed provides a powerful methodology for the development of materials and microwave devices.

1. Introduction

Electrically tunable barium strontium titanate ($Ba_xSr_{1-x}TiO_3$) perovskite films, hereafter referred as BSTO, of the general stoichiometry ABO_3 (A and B cations of different sizes) are of strong interest due to their appealing electrical properties.[1-4] As the films possess high relative permittivity ε_r, low loss tangent tanδ and high tunability, BSTO have been widely investigated for dynamic random access memory (DRAM),[5] high voltage capacitors,[6] tunable filters[7], microwave phase shifters [8, 9]etc. Although semiconductors, liquid crystals, optical fibers, magnets, ceramics and ceramic nanocomposites [10] and many other alternative materials have been used for tunable devices, ferroelectrics in their paraelectric phase are far more effective, as they exhibit high dissipation factor (Q), consume negligible power, operate at high speeds and can be tuned with relatively low DC bias (<30 V).[11] Among the aforementioned applications, BSTO-based microwave phase shifting devices are extremely desirable, because they have compact structure, exhibit low loss and are easy to tune. For this kind of microwave devices, the tunability and dielectric loss are the two critical parameters to determine the overall performance of the devices. On the one hand, the developed dielectrics phase shifters are expected to exhibit wide tuning range, on the other hand, the overall insertion loss of the devices should be as low as possible. But the two properties of the BSTO are generally at odds. In microwave and millimetre wave regime, at room temperature the loss tangent is proportional to the frequency according to the equation: $\tan\delta \propto \omega\varepsilon_r^{3/2}T^2$, where ε_r is the relative permittivity of the ferroelectrics materials.[11] Lower loss tangent typically denotes a smaller relative permittivity of the material,

[a] Department of Chemistry, University of Southampton, Southampton, SO17 1BJ, UK. E-mail: B.E.Hayden@soton.ac.uk
[b] Department of Electronics and Computer Science, University of Southampton, Southampton, SO17 1BJ, UK. E-mail: chdg@ecs.soton.ac.uk
[c] Ilika Technologies, Kenneth Dibben House, Chilworth Science Park, Southampton SO167 NS
[d] School of Engineering and Digital Arts, University of Kent, Canterbury, CT2 7NT, UK
[e] Department of Materials Science and Engineering, University of Sheffield, Sheffield, S1 3JD, UK

† Footnotes relating to the title and/or authors should appear here.
See DOI: 10.1039/x0xx00000x

that leads to a limited tuning range of the devices based on such kind of dielectric layers.[12] By contrast, it has been observed that when the dielectric constant and tunability increases, the dielectric loss increases as well, due to the fact that when a DC electric field is applied, the extrinsic losses dominate[11]. The same trend is followed by the tuning range and the insertion loss, thus it is challenging to meet both requirements for a BSTO based phase shifter.

Various studies have taken place to optimize the properties of the tunable dielectric thin films and it has been observed that many factors affect the quality of the dielectric thin film. These factors include the temperature of the deposition, the film's thickness,[13] the substrate[14, 15] possible induced stress[16] and strain.[17] Improvement of the dielectric properties can also be achieved by post annealing at oxygen, [18] or as it has recently been discussed, by inserting a bimetallic layer in thin films. [19] In particular for the perovskite materials, the relative ratio of the cations on the A and the B site of the BSTO can significantly affect both the tunability and dielectric loss of the films.[20] Moreover, oxygen vacancies have been proved to be of great importance for the dielectric properties of perovskites and the performance of the perovskite-based devices.[21-23] Pervez et al [9] investigated the influences of A to B ratio, and found that increasing the A/B ratio could lead to lower loss tangent of the films but the ε_r also decreased, as well as the tunability of the materials. Attar et al.[24] doped the $Ba_{0.5}Sr_{0.5}TiO_3$ with Bi and obtained a high dielectric constant up to 1040. Su et al.[25] recently found when the Mg doping concentration (<2 mol%) increased, significant suppression of permittivity and losses can be observed.

Doubly charged acceptor (A^{2+}) ions on the B-site (A_{Ti}'') such as Mg^{2+} act as acceptor dopants according to the general equation:

$$AO \leftrightarrow A_{Ti}'' + O_O + V_O^{\bullet\bullet} \quad (1)$$

A_{Ti}'' are considered to compensate for native levels of $V_O^{\bullet\bullet}$ in titanates (suppressing the formation of Ti^{3+}) and to also reduce their mobility. Generally however, doping on the B site of titanate-based perovskite films is carried out with variable valence elements such as Fe, Co, Mn and Cr. These transition metal ions compensate for native levels of $V_O^{\bullet\bullet}$ but equally can exist in higher valence (iii and iv) states according to the following[26-28]

$$AO_{1.5} \leftrightarrow A_{Ti}' + {}^3/_2O_O + {}^1/_2V_O^{\bullet\bullet} \quad (2)$$

$$AO_2 \leftrightarrow A_{Ti} + 2O_O \quad (3)$$

They can therefore adapt to local stoichiometric variations and help reduce dielectric loss.

Mn doped BSTO (<2 mol%) thin films grown on MgO substrates by Pulsed Lased Deposition (PLD), have shown low frequency dielectrics tunability of 80 % and very low insertion losses (1.5 dB) at 30 GHz.[29] No high frequency tunability or phase angle of the CPW was determined though. As the stoichiometry of the films has a significant influence on the properties of the perovskite films, to develop high performance microwave devices with these materials, a systematic study should be conducted to evaluate the influences of the composition, and BSTO films have to be evaluated at the high operating frequencies.

There are many ways to deposit perovskite films with ABO_3 structure, such as sputtering,[17] PLD,[30] Metal Organic Chemical Vapour Deposition (MOCVD),[31] sol-gel method[20] and Molecular Beam Epitaxy (MBE).[4, 32, 33] In this paper, a modified MBE system was used to synthesize the thin films. We report a systematic study of coplanar waveguide (CPW) structure microwave phase shifters with Mn doping BSTO ceramics. The cation ratios and cation substitutions of the BSTO films are varying and mechanisms of chemical compositions on the dielectric properties and the performance of the devices are discussed. The very high operating frequency (>10 GHz) of the CPW structure phase shifters based on Mn-BSTO is attributed to the low losses and good rates of tunability with the application of an external electric field above 10 GHz.

2. Experimental details

Mn-BSTO thin films preparation

Mn doped $Ba_xSr_{1-x}TiO_3$ thin films have been deposited on Pt-coated substrates ($Pt/TiO_2/SiO_2/Si$) with high throughput Physical Vapor Deposition (PVD) using a modified MBE system from DCA Instruments.[34] The synthesis protocol is based on a slightly modified method as reported in more detail elsewhere.[4] Ba (Alfa Aesar: 99.9 %,) and Sr pieces (Alfa Aesar: 99 %), and Mn flakes (GoodFellow: 99.95%) were contained in Ta, PBN and Al_2O_3 crucibles respectively, and evaporated using Knudsen cells (from DCA instruments). Ti pellets (99.995 % supplied from Testbourne) were placed on a graphite crucible and evaporated with a 40 cc electron gun from Telemark. The substrates were heated to 640 ℃. Atomic oxygen was supplied through a RF atom source (HD25, Oxford Applied Research) using 545 W of RF power and an oxygen flow rate of 1.02 ml/min. The compositional spread is achieved by wedge shutters[34] that are placed above the beam of the evaporating material. A deposition time of 55 mins resulted in the average thickness of 260 nm. Variations in the thickness of the films are expected due to the compositional spread along the surface of the film and the evaporation process. To improve the crystallinity of the thin films, after the deposition they were subsequently annealed in a tube furnace at 650 °C for 30 min under a N_2 flow.

Mn-BSTO thin films characterization

The elemental analysis of the fabricated films was carried out using Scanning Electron Microscopy (SEM) and Energy Dispersive X-Ray Spectroscopy (EDX) using a Tesca Vega 3 equipped with an EDX detector XMax 50 from Oxford Instruments whereas the crystal structure was investigated by X-Ray diffraction patterns using a Bruker D8 diffractometer equipped with an Incoatec microsource Cu Kα and GADDS detector. The low frequency (1 kHz-100 kHz) measurements of the dielectric constant and loss were carried out on Mn-BSTO thin films of average thickness 210 nm, using a LCR bridge

(Hewlett Packard 4284A) with an AC voltage of 100 mV. An array of 14 × 14 of 290 µm diameter platinum top electrodes of 2 mm pitch between them was deposited with RF sputtering resulting in the formation of 196 parallel plate capacitors of different BSTO compositions.

Phase Shifters fabrication and characterization

The devices were fabricated on 150 mm high resistive (30 Ω·cm to 60 Ω·cm) silicon substrates with a 500 nm thermalized SiO_2 insulating layer. The bottom electrodes, consisting of 10/300 nm refractory Ti/Pt layer, were patterned by a standard lift-off process and sputtered on the SiO_2 before the synthesizing of the BSTO layer. Then, using a photoresist mask, the BSTO layer was etched in 7:1 HF etchant for 2 minutes to selectively define the active BSTO layer. After that, a 250 nm Al layer was thermally evaporated on the substrates and the top electrodes of the devices were defined by photolithography and wet etching. The samples were immersed in Al etchant for about 6 minutes to obtain the desired patterns. The reflection- (S_{11}), transmission- (S_{21}) characteristics, and the phase angle (φ) of the devices were measured using a Cascade semi-automatic microwave probe station with GSG coplanar probes connected to an Agilent E8361A vector network analyzer, and varying DC biasing voltage from 0-10 V supplied by a separate power source.

3. Results and discussion

Structure and dielectric properties of thin films

The crystal structure of the fabricated thin films has been investigated by X-Ray diffraction. Figure 1 shows typical X-Ray patterns obtained from areas of the thin film which correspond to different cationic stoichiometry. The structures of the fabricated thin films correspond to compositions near the ideal substituted perovskite $Ba_xSr_{(1-x)}Ti_yMn_{(1-y)}O_3$. The addition of Mn in such low percentages is not expected to result in shift of the Bragg peaks, therefore the observed peaks are nicely matched with the Bragg reflections of the tetragonal $Ba_{0.77}Sr_{0.23}TiO_3$ compound (ICDD database- PDF card 00-044-0093) shown as vertical red tick marks. The relative intensities of the peaks are similar to those expected for polycrystalline ceramics and therefore we conclude that the films are mainly composed of randomly oriented grains. The upper layers of substrate had SiO_2/Pt. The peak around 24 degrees, indicated in the figure with an asterisk, is attributed to the substrate as it matches with the (100) reflection of SiO_2 (silicon oxide zeolite, PDF card 00-045-0112). Morerover, the reflection at 39.1 degrees (111) of the perovskite overlaps with the (111) of the Pt (39.3 degrees). In order to check the dielectric properties and the tunability of the Mn-BSTO thin films at low frequencies, measurements of the dielectric constant and dielectric loss were carried out at frequencies of 1, 10 and 100 kHz versus DC applied voltage ranging from 0 to 9 V, corresponding to a maximum electric field of 450 kV/cm, as shown in Fig 2.

The thin films exhibited high dielectric constant ε'_r= 523 and low dielectric loss, tanδ= 0.048, at 0 electric field, which could be tuned to ε'_r = 218 and tanδ = 0.02, respectively, at the maximum

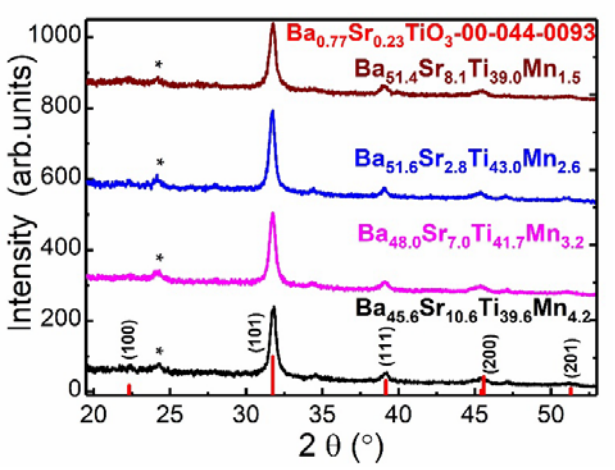

Fig.1 X-Ray diffraction pattern of the Mn-doped BSTO thin films at different areas of the film and identification with the reflections of the $Ba_{0.77}Sr_{0.23}TiO_3$ compound shown with the red tick marks as obtained from the PDF card 00-044-0093.

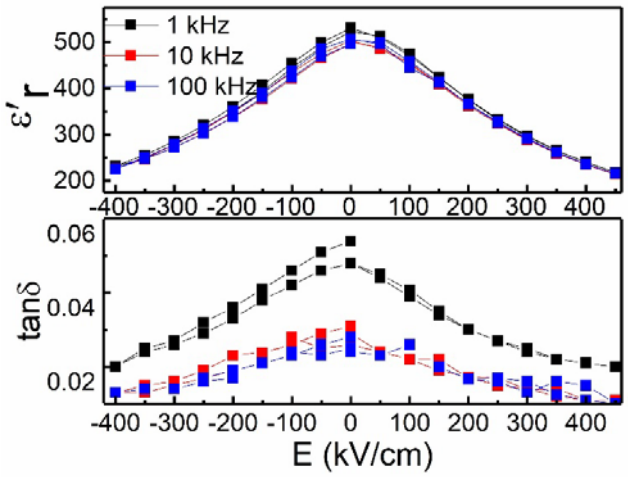

Fig.2: Dielectric Constant (ε'_r) and dielectric loss (tanδ) of Mn-BSTO thin films measured at 1, 10 and 100 kHz under electric fields of 0-450 kV/cm. The excitation voltage from the LCR Bridge was 100 mV.

applied (450 kV/cm) at the frequency of 1 kHz. At higher frequencies of 100 kHz, the dielectric constant ranges from 500 to 214, the tanδ decreases from 0.024 to 0.01 as the field increases from 0 to 450 kV/cm. The change of the dielectric constant corresponds to a remarkable tunability of 58.3 % for 1 kHz and 57.3 % at 100 kHz. A typical graph of the dielectric constant and loss, of a Mn-BSTO thin film (Mn: 3.11%) versus the DC applied electric field is presented in Figure 2. One profound characteristic is the reduction of the dielectric loss at 100 kHz, in comparison with the dielectric loss obtained for the

lower frequencies of 1 and 10 kHz. These results indicate the possible improvement of the dielectric properties of BSTO thin films at higher frequencies due to the Mn-doping, as earlier studies on undoped BSTO films[4] showed comparable values of dielectric properties at frequencies up to 1 kHz.

Waveguide structures and devices' performance

A few structures are suitable to develop BSTO based phase shifters, such as the loaded transmission lines,[8, 35] coupled microstrip lines[36] and the interdigital transducers (IDTs).[37, 38] In this paper, a coplanar waveguide (CPW) structure phase shifter is proposed in which the dielectric is sandwiched between ground and signal line. Fig. 3(a) shows the fabricated BSTO co-planar waveguide phase shifter. The effective unit of the phase shifter is a varactor with a vertical sandwich structure as shown schematic in Figure 3 (b). Active area of the varactor used is 5 µm × 10 µm. Figure 3 (c) shows the SEM cross-sectional image of the structure with a BSTO/Pt/SiO_2/Si stack, whereas Figure 3 (d) provides a zoom in on the Al/BSTO/Si stack. The thickness of the dielectric layer is ~260 nm and the individual BSTO grains can be resolved, confirming the polycrystalline nature of the films.

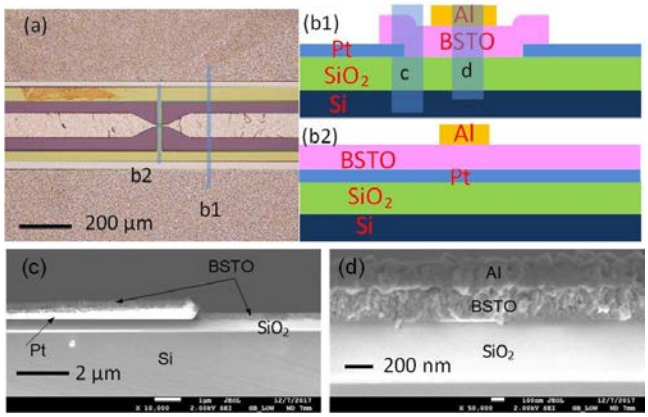

Fig. 3 (a) Micrograph of the fabricated BSTO co-planar waveguide phase shifter (b1, b2) Schematic drawing of the cross-section of the CPW as indicated in blue lines in (a). (d), SEM cross-sectional image of the CPW corresponding to the shaded regions in (b1).

In order to investigate the dielectric properties of the fabricated varactors the reflection (S_{11}) and transmission (S_{21}) coefficients have been measured. Figure 4 presents data measured on the area of the varactor where the dielectric thin film has the stoichiometry $Ba_{51.1}Sr_{7.4}Ti_{39.5}Mn_{2.0}O_3$. Measurements were obtained in the frequency range of 0-20 GHz and at various electric fields from 0 kV/cm to 385 kV/cm corresponding to applied voltages from 0 to 10 V. Figure 4 (a) shows the variation of the return loss with the applied voltage versus the frequency. The device shows a return loss of -12.3 dB at 10 GHz for 0 kV/cm. At 385 kV/cm (10 V applied voltage) the return loss reduces to -17.5 dB, implying the optimization of the impedance matching of the CPW structure.

The improvement of the matching leads to the optimization of the transmission characteristics of the device as well, as shown in Figure 4(b). The insertion loss (IL) decreases continually with increasing biasing voltage, to 3.3 dB with 385 kV/cm applied field, from originally 3.6 dB loss at 0 kV/cm. Figure 4(c) represents the continual variations of the phase angle (ϕ) of the device in respect with the frequency. Overall, ϕ decreases linearly when frequency increases, and with higher operating frequency, the discrepancy of the device under different electric field becomes more significant. Typically, the phase angle of the device will recover to the original value when removing the electric field, as shown in Figure 4(d).

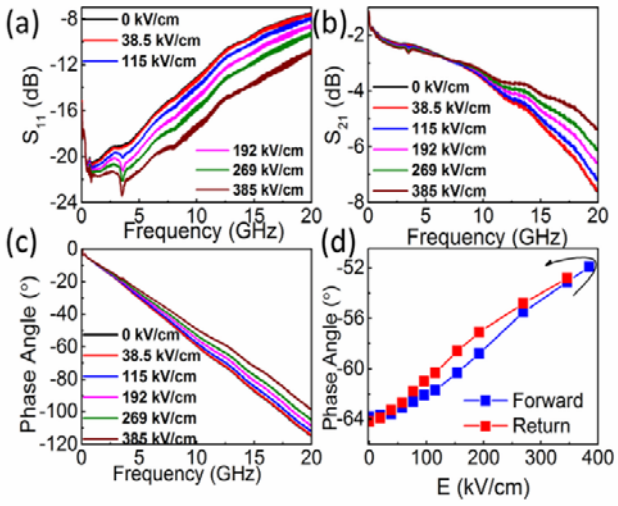

Fig. 4 Measured results of CPW phase shifters with varying DC bias voltage from 0 to 10 V: (a) Return loss; (b) Insertion loss; (c) Continual phase angle shifting; (d) Retention curve of phase angle shifting with forward and return DC biasing.

Figure 5(a) shows the High Frequency Structure Simulator (HFSS) model of the phase shifter unit cell for simulation. The active area of the phase shifter is 5 µm × 10 µm, the structure parameters for the simulation model were chosen according to the experimental details, which have been illustrated in the previous section. Based on the results of C-V measurement, the loss tangent (tanδ) of the BSTO film was fixed at 0.015, while the dielectric constant (ε'_r) varies from 150 to 200, corresponding to an electric field from 0 kV/cm to 154 kV/cm. Figure 5 (b) shows a comparison of the measured transmission curves with the simulated results, showing a good agreement with each other. For both the simulated and measured spectra, the IL increases with increasing operating frequency. For frequency lower than 10 GHz, the simulated IL (<3 dB) is slightly lower than the experimental data, and when the operating frequency continues to increases, the model exhibit higher loss. Figure 5(c) shows a comparison of the measured phase angle varying spectra with the simulated results. The phase angle of the device decreases approximately linearly with increasing frequency. The discrepancy between the simulated and

measured results is mainly attributed to the neglect of the variation of the loss tangent with frequency. In the HFSS model tanδ is fixed, while in practice, this figure is varying with frequency; this needs to be optimized in future work. Nevertheless, it is clearly shown that when ε'_r increases from 150 to 200, the phase tuning is small (~ 4°) in both simulated and experimental results.

The influence of BSTO compositions on phase shifter performances is investigated. Fig. 6 shows the 3 × 3 BSTO array, the X and Y coordinates denote different positions on the 35 mm × 35 mm sample. The inset table of Figure 6 shows the details of the average cationic distribution and the electrical performances of the relevant phase shifters. A notable characteristic of the throughput data is that it enables us to compare phase shifters using similar compositions of

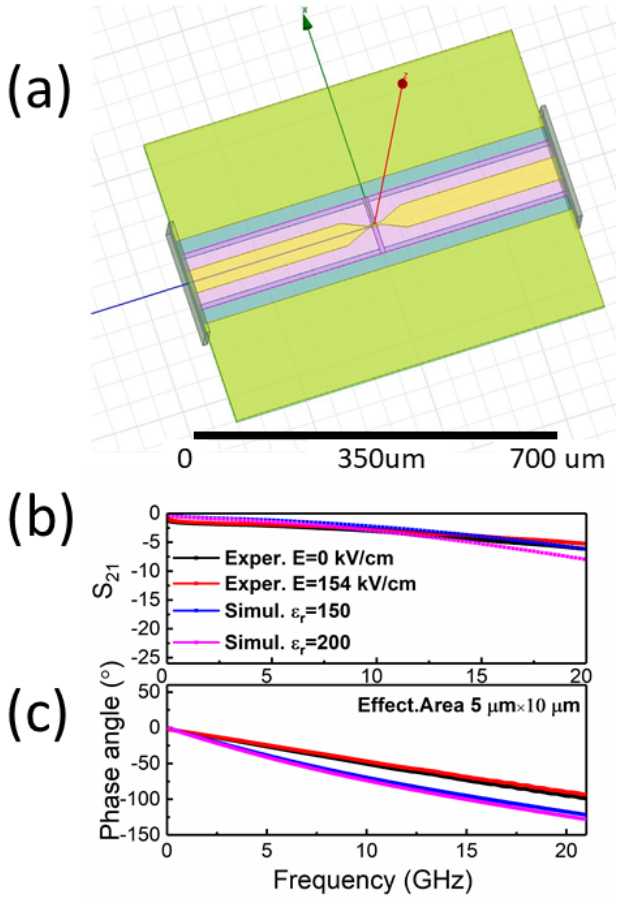

Fig.5: (a) HFSS model for the co-planar waveguide phase shifter.(b)Experimental and simulated graphs of the transmission at zero and maximum field (c) Experimental and simulated graphs of the phase shift angle between zero and maximum field.

BSTO films. Specifically, the above table summarizes the variations of the insertion loss and phase angle shifting of the phase shifters on different positions of the sample with varying BSTO compositions. For example, along with the X1 column, when the position change from Y1 to Y3 (BSTO composition varies from $Ba_{0.46}Sr_{0.1}Ti_{0.4}Mn_{0.04}O_3$ to $Ba_{0.49}Sr_{0.11}Ti_{0.38}Mn_{0.02}O_3$), generally, the insertion loss of the phase shifter decreases, denoting the decreasing intrinsic loss (*tanδ*) of the films, which will lead to optimized transmission characteristics of the devices. However, as can be read from table of Figure 6, the phase shift angle decreases as well; the differential phase angle reduces from 4.05˚ to 2.32˚ with a small biasing voltage of 5 V, which is more

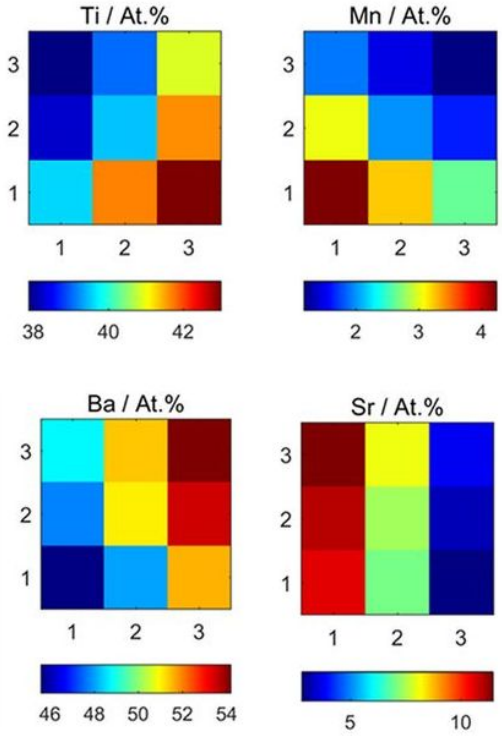

X	Y	Ba (%)	Sr (%)	Ti (%)	Mn (%)	S_{21} (dB) 10 GHz	Phase Angle (°) at 192 kV/cm	Figure of Merit (°/dB)
1	1	45.6	10.6	39.6	4.3	3.1	2.3	0.7
1	2	47.8	11.0	38.2	3.0	3.4	3.0	0.9
1	3	48.7	11.5	37.9	1.9	3.2	4.0	1.3
2	1	48.0	7.0	41.7	3.3	3.3	3.2	1.0
2	2	51.1	7.4	39.5	2.0	3.5	4.3	1.2
2	3	51.4	8.1	39.0	1.5	3.8	5.1	1.4
3	1	51.5	2.8	43.0	2.6	3.2	3.6	1.1
3	2	53.5	3.2	41.6	1.6	3.8	4.9	1.3
3	3	54.2	3.8	40.9	1.2	4.1	4.9	1.2

Fig.6: Upper panel: Array (3×3) maps of the cationic characteristics of the Mn-BSTO films synthesized on a 35 mm × 35 mm substrate. Variations of Ti, Mn, Ba and Sr concentrations. Lower panel: Inset table summarizes the atomic percentage details ratio of each catio in different positions of the film.The results are shown in respect with the original insertion loss for the phase shifter at 10 GHz and the variation of the phase angle with 192 kV/cm applied electric field.

significant than the variation of insertion loss. We can obtain similar results for devices along column X2 and X3. According to the results presented in table of Figure 6, the waveguide with the best RF

performance is the one with the phase angle of 5.1 (°) which corresponds to the BSTO composition $Ba_{51.4}Sr_{8.1}Ti_{39.0}Mn_{1.5}$.

In this research, we doped the BSTO films with Mn, demonstrating that the insertion loss of the devices is inversely proportional to the Mn doping ratio, while the phase shift exhibits opposite trend. Our results are in agreement with dielectric studies carried out in Mn-doped BSTO ceramics, where it has been found that the addition of Mn decreased the dielectric loss but also decreases the tunability. This effect has been rationalised in terms of the deterioration of the long range ferroelectric order with the addition of the Mn. [39] The increase in the tunability of the devices typically dominates over the drawbacks of increasing loss for phase shifter applications, so a perovskite film with higher tunability is usually preferred. Note that the ideal stoichiometry for the perovskite structure is characterized by equivalent percentages on the A and B site in $(Ba_x, Sr_{(1-x)})(Ti_{(y)}, Mn_{(1-y)})O_3$. The dielectric films studied had an excess of the cation on the A site (sum of Ba and Sr was higher around 5-9 %) and the B-site (sum of Ti and Mn) was lower similarly by a 5-9 %. Nevertheless, one can observe that the perovskite structure is not affected. This is evident by the X-Ray diffraction pattern (Figure 1) which shows that the crystal structure of the thin films can be identified upon the perovskite Bragg reflections. Furthermore the dielectric tunability is notably large (58 %), the dielectric constant is high (exceeding 500 for 0 kV/cm of electric field) the dielectric loss is low (less than 3-6 % for 1-100 kHz and 3.2 dB at 10 GHz for the coplanar waveguides). Yet, the possibility of enhancing the desired dielectric properties by the modification of the cationic percentage and composition gives a broader potential to the research of the BSTO thin films with high frequency applications. So far the prevailing model for explaining the tunability of the BSTO thin films is the hardening of the soft phonon mode. [40, 41] However, to gain a better insight on the effects of the substitution of the Ti with the Mn and correlate the finding with the mechanism of tunability and the microwave characteristics of the obtained devices, a more extensive high throughput study is required controlling the composition, crystallinity, morphology and their relationship with dielectric properties.

4. Conclusions

Mn doped BSTO films have been synthesized using high throughput evaporative PVD. Co-planar waveguide phase shifters with single varactor cell incorporating these thin films have been fabricated, and the electrical properties of the phase shifters characterized. The devices are shown to operate at over 10 GHz with a low insertion loss of ~3.2 dB. The devices are tunable with applied voltage. At a small biasing voltage of 10 V, over 12° phase angle shifting can be obtained with excellent transmission characteristics. An HFSS based model is used to evaluate the phase shifters' performance. The simulation results are consistent with experiments. The impact of (Ba, Sr)(Ti, Mn)O_3 compositions on device performances is studied. It is found that the tunability and the overall loss of the phase shifters are at odds. Slight change of the stoichiometry of the perovskite films can lead to significant changes for both properties of the phase shifters. The phase angle of the devices is most susceptible to compositional variation. We demonstrate the potential of a combinatorial synthetic methodology combined with the appropriate design of phase shifters for high throughput screening for the optimisation of tunable materials with low loss for high frequency applications.

Conflicts of interest

There are no conflicts to declare.

Acknowledgements

The authors would like to acknowledge EPSRC funding (EP/N032470/1). The synthesis of the BSTO thin films was carried out in collaboration with Ilika plc with the help of Dr Sergey Yakovlev and Mr. Matthew Huttchins.

Notes and references

1. H. Bouyanfif, J. Wolfman, M. E. Marssi, Y. Yuzyuk, R. Bodeux, M. Gervais and F. Gervais, *Journal of Applied Physics*, 2009, **106**, 034108.
2. Seokmin Hong, Heungjin Bak, Ilsin An and Kyung K. Ok, *Japanese Journal of Applied Physics*, 2000, **39**, 1796.
3. S. Ito, H. Funakubo, I. P. Koutsaroff, M. Zelner and A. Cervin-Lawry, *Applied Physics Letters*, 2007, **90**, 142910.
4. A. David, S. Guérin, B. E. Hayden, R. Noble, J.-P. Soulié, C. Vian, I. P. Koutsaroff, S. i. Higai, N. Tanaka, T. Konoike, A. Ando, H. Takagi, T. Yamamoto, T. Fukura and H. Ieki, *Crystal Growth & Design*, 2014, **14**, 523-532.
5. D. E. Kotecki, J. D. Baniecki, H. Shen, R. B. Laibowitz, K. L. Saenger, J. J. Lian, T. M. Shaw, S. D. Athavale, C. Cabral, P. R. Duncombe, M. Gutsche, G. Kunkel, Y. J. Park, Y. Y. Wang and R. Wise, *IBM Journal of Research and Development*, 1999, **43**, 367-382.
6. T. Samoilova, M. Gaidukov, A. Tumarkin, A. Gagarin, A. Altynnikov and A. Kozyrev, *Journal of Applied Physics*, 2014, **115**, 204103.
7. A. Tombak, J. P. Maria, F. T. Ayguavives, J. Zhang, G. T. Stauf, A. I. Kingon and A. Mortazawi, *IEEE Transactions on Microwave Theory and Techniques*, 2003, **51**, 462-467.
8. A. S. Nagra and R. A. York, *IEEE Transactions on Microwave Theory and Techniques*, 1999, **47**, 1705-1711.
9. N. K. Pervez, P. J. Hansen and R. A. York, *Applied Physics Letters*, 2004, **85**, 4451-4453.
10. M. Airimioaei, M. T. Buscaglia, I. Tredici, U. Anselmi-Tamburini, C. E. Ciomaga, L. Curecheriu, A. Bencan, V. Buscaglia and L. Mitoseriu, *Journal of Materials Chemistry C*, 2017, **5**, 9028-9036.
11. S. Gevorgian, *Ferroelectrics in Microwave Devices, Circuits and Systems*, Springer, London, 2009.
12. A. K. Tagantsev, V. O. Sherman, K. F. Astafiev, J. Venkatesh and N. Setter, *Journal of Electroceramics*, 2003, **11**, 5-66.
13. C. Basceri, S. K. Streiffer, A. I. Kingon and R. Waser, *Journal of Applied Physics*, 1997, **82**, 2497-2504.
14. J. H. Hao, Z. Luo and J. Gao, *Journal of Applied Physics*, 2006, **100**, 114107.
15. A. Tkach, O. Okhay, I. M. Reaney and P. M. Vilarinho, *Journal of Materials Chemistry C*, 2018, **6**, 2467-2475.
16. T. M. Shaw, Z. Suo, M. Huang, E. Liniger, R. B. Laibowitz and J. D. Baniecki, *Applied Physics Letters*, 1999, **75**, 2129-2131.

17. T. R. Taylor, P. J. Hansen, B. Acikel, N. Pervez, R. A. York, S. K. Streiffer and J. S. Speck, *Applied Physics Letters*, 2002, **80**, 1978-1980.
18. S. Yu, L. Li, D. Xu, H. Dong and Y. Jin, *Journal of Materials Chemistry C*, 2014, **2**, 9683-9688.
19. P.-W. Chi and D.-H. Wei, *Journal of Materials Chemistry C*, 2017, **5**, 1394-1401.
20. T. R. Taylor, P. J. Hansen, N. Pervez, B. Acikel, R. A. York and J. S. Speck, *Journal of Applied Physics*, 2003, **94**, 3390-3396.
21. Y.-K. Choi, T. Hoshina, H. Takeda, T. Teranishi and T. Tsurumi, *Applied Physics Letters*, 2010, **97**, 212907.
22. X.-X. Huang, T.-F. Zhang, X.-G. Tang, Y.-P. Jiang, Q.-X. Liu, Z.-Y. Feng and Q.-F. Zhou, *Scientific Reports*, 2016, **6**, 31960.
23. E. Enriquez, A. Chen, Z. Harrell, P. Dowden, N. Koskelo, J. Roback, M. Janoschek, C. Chen and Q. Jia, *Scientific Reports*, 2017, **7**, 46184.
24. A. Sadeghzadeh Attar, E. Salehi Sichani and S. Sharafi, *Journal of Materials Research and Technology*, 2017, **6**, 108-115.
25. B. Su and T. W. Button, *Journal of Applied Physics*, 2004, **95**, 1382-1385.
26. K.-T. Kim and C.-I. Kim, *Thin Solid Films*, 2005, **472**, 26-30.
27. A. Jasik, S. M. Kaczmarek, K. Matyjasek, J. Barczynski and M. Berkowski, *Phase Transitions*, 2013, **86**, 230-237.
28. L. B. Kong, S. Li, T. Zhang, J. Zhai, F. Y. C. Boey and J. ma, *Electrically Tunable Dielectric Materials and Strategies to Improve Their Performances*, 2010.
29. Z. Yuan, Y. Lin, J. Weaver, X. Chen, C. L. Chen, G. Subramanyam, J. C. Jiang and E. I. Meletis, *Applied Physics Letters*, 2005, **87**, 152901.
30. M. Santosh, M. Lacotte, A. David, B. Ph, C. Grygiel, D. Pravarthana, G. S. Rohrer, P. A. Salvador, P. Padhan, U. Lüders, W. Junling and W. Prellier, *Journal of Physics D: Applied Physics*, 2017, **50**, 235301.
31. C. S. Hwang, S. Y. No, J. Park, H. J. Kim, H. J. Cho, Y. K. Han and K. Y. Oh, *Journal of The Electrochemical Society*, 2002, **149**, G585-G592.
32. B. E. Hayden and S. Yakovlev, *Thin Solid Films*, 2016, **603**, 108-114.
33. M. S. B. Darby, S. Guerin, B. E. Hayden, H.-J. Schreiner and S. Yakovlev, *Journal of Applied Physics*, 2013, **113**, 014104.
34. S. Guerin and B. E. Hayden, *Journal of Combinatorial Chemistry*, 2006, **8**, 66-73.
35. R. Han-cheol, M. Seung Eon, L. Su-jae, K. Min-hwan, K. Young-tae and K. Kwang-young, *Japanese Journal of Applied Physics*, 2004, **43**, 6746.
36. S. Sheng and C. K. Ong, *Journal of Applied Physics*, 2012, **111**, 044506.
37. L. Lai, Y. Xu, Y. Ren, H. Gao, X. Wang, J. Zhu, Y. He and X. Zhu, *Journal of Materials Science: Materials in Electronics*, 2017, **28**, 5718-5724.
38. C. M. Andersson, N. Ejebjork, A. Henry, S. Andersson, E. Janzen, H. Zirath and N. Rorsman, *IEEE Electron Device Letters*, 2011, **32**, 788-790.
39. J. Zhang, J. Zhai and X. Yao, *Scripta Materialia*, 2009, **61**, 764-767.
40. I. A. Akimov, A. A. Sirenko, A. M. Clark, J. H. Hao and X. X. Xi, *Physical Review Letters*, 2000, **84**, 4625-4628.
41. R. Waser, *Nanoelectronics and Information Technology*, Wiley, 2012.